Coexistence of topological nontrivial and spin-gapless semiconducting behavior in $MnPO_4$: A composite quantum compound

Chia-Hsiu Hsu,[1,*] P. C. Sreeparvathy,[2,*] Chanchal K. Barman,[2] Feng-Chuan Chuang,[1,3,4,†] and Aftab Alam[2,‡]

[1]*Department of Physics, National Sun Yat-sen University, Kaohsiung 80424, Taiwan*
[2]*Department of Physics, Indian Institute of Technology Bombay, Powai, Mumbai 400076, India*
[3]*Department of Physics, National Tsing Hua University, Hsinchu 30043, Taiwan*
[4]*Physics Division, National Center for Theoretical Sciences, Hsinchu 30013, Taiwan*

(Received 31 December 2020; accepted 29 April 2021; published 19 May 2021)

Composite quantum compounds (CQC) are a classic example of quantum materials, which host more than one apparently distinct quantum phenomenon in physics. Magnetism, topological superconductivity, Rashba physics, etc. are a few such quantum phenomenon, which are ubiquitously observed in several functional materials and can coexist in CQCs. In this paper, we use *ab initio* calculations to predict the coexistence of two incompatible phenomena, namely topologically nontrivial Weyl semimetal and spin-gapless semiconducting (SGS) behavior, in a single crystalline system. SGS belongs to a special class of spintronics material, which exhibits a unique band structure involving a semiconducting state for one spin channel and a gapless state for the other. We report such a SGS behavior in conjunction with the topologically nontrivial multi-Weyl fermions in $MnPO_4$. Interestingly, these Weyl nodes are located very close to the Fermi level with the minimal trivial band density. A drumhead-like surface state originating from a nodal loop around Y point in the Brillouin zone is observed. A large value of the simulated anomalous Hall conductivity (1265 $\Omega^{-1}cm^{-1}$) indirectly reflects the topological nontrivial behavior of this compound. Such co-existent quantum phenomena are not common in condensed matter systems and hence it opens up a fertile ground to explore and achieve newer functional materials.

DOI: 10.1103/PhysRevB.103.195143

I. INTRODUCTION

Coexistence of two or more complementary quantum phenomenon in a single material often provides a fertile ground to explore the fundamental correlation between these different processes in physics. Apart from basic science, such amalgamation of different quantum properties can also open the door for potential technological applications. The compounds, which show such combined quantum properties are called the composite quantum compounds (CQC) [1]. To date, only a handful of such CQCs have been realized, e.g., topological superconductivity involving superconductivity and topology [2,3] topological axion insulator between topology and magnetism, which are currently one of the emerging fields of interest [4,5].

Spintronics and topological nontrivial band ordering are two distinct quantum phenomenon, which can be connected via the common prerequisite of spin-orbit coupling (SOC). There are LiGaGe-type polar compounds where ferroelectricity and topological insulator (TI) phases are coupled together via the presence of strong SOC and broken inversion symmetry [6]. Another classic example of CQC is BiTeI, which shows coexistence of TI phase and large Rashba spin splitting under the influence of external pressure [7]. Though there exist some reports on few CQCs, the hunt for newer class with more exotic complimentary quantum properties is still ongoing.

In this paper, we propose a material platform that can simultaneously showcase the existence of nontrivial multiple Weyl nodes and/or nodal line along with the so-called spin-gapless semiconducting (SGS) behavior. SGS are new states of quantum matter, which are characterized by a unique spin-polarized band structure [8]. Unlike conventional semiconductors or half-metallic ferromagnets, they carry a finite band gap for one spin channel and close (zero) gap for the other and thus are useful for tunable spin transport applications. It is one of the latest classes of materials considered for spintronic devices. A few of the several advantages of SGSs include (i) minimal amount of energy required to excite electrons from valence to conduction band due to zero gap, (ii) availability of both charge carriers, i.e., electrons as well as holes, which can be 100% spin-polarized simultaneously, (iii) high Curie temperature for a large number of them [9–11]. Several number of SGS materials have been predicted in the last few years using both theoretical as well as experimental tools [12]. Weyl semimetals (WSM), on the other hand, are also known to show fascinating transport signatures e.g., anomalous Hall effect (AHE), which describes the transverse voltage drop resulting from an applied longitudinal electric field. Contrary to classical Hall effect under applied magnetic field, a momentum-dependent fictitious magnetic field (Berry curvature) causes the AHE in Weyl semimetals [13,14]. As such, a magnetic Weyl semimetallic system could be an ideal

*These two authors have contributed equally to this work.
†fchuang@mail.nsysu.edu.tw
‡aftab@iitb.ac.in

platform to achieve a Berry curvature-induced AHE because Weyl nodes are source (sink) of large Berry flux in this case. Another interesting feature is the large magnitude of anomalous Hall conductivity (AHC) in systems that host Weyl-type band crossings near the Fermi level [15]. For example, a large value of AHC (= 1130 Ω^{-1} cm^{-1}) is reported for $Co_3Sn_2S_2$ [16,17]. Co_2MnAl [18] is another example which show a giant value of AHC, around 1277 Ω^{-1} cm^{-1}, at room temperature. Several other magnetic compounds including Heusler alloys [15,19] are also found to show such Weyl points and consequently large AHC [20–22]. The density functional theory calculations play a crucial role in discovering several topological semimetals. Yet, finding an ideal candidate material where Weyl/Dirac nodes lie close to the Fermi level (E_F) is always challenging.

The purpose of the present paper is to report $MnPO_4$ as the first CQC, which exhibit both SGS and multi-Weyl semimetal behavior. Unlike the conventional WSM, this compound shows four pairs of Weyl nodes in its band structure, all of which are closely located to E_F, with minimal trivial band density. It shows a significantly large AHC of 1265 Ω^{-1} cm^{-1}, similar to other reported WSM. Being the first of its kind, $MnPO_4$ is expected to enjoy all the advantages of the two unique quantum properties, as explained above.

II. COMPUTATIONAL DETAILS

The Vienna *ab initio* Simulation Package (VASP) [23,24] based on density functional theory (DFT) has been used to carry out the simulation. We used generalized gradient approximation by Perdew-Burke-Ernzerhof (PBE) [24] to treat exchange and correlation. To enforce the localization of the Mn-d electrons, we perform PBE + U calculation [25] with a Hubbard U (= 3.9 eV) introduced in a screened Hartree-Fock manner. Justification for the use of this U value is given in the Supplemental Material (SM) [33]. Plane wave basis set using projector augmented wave (PAW) [26] method was used with an energy cutoff of 520 eV. Brillouin zone (BZ) integrations were performed using a 12 × 12 × 10 k mesh. Total energy was converged up to 10^{-6} eV. The spin-orbit coupling (SOC) effect was included. Phonon frequencies were calculated using density functional perturbation theory (DFPT) using phonopy [27]. Maximally localized Wannier functions (MLWF) [28–30] were used to construct a tight binding model to closely reproduce the bulk band structure. WANNIERTOOLS package [31] was employed to simulate the topological properties, and AHC.

III. RESULTS AND DISCUSSION

A. Crystal structure and stability

$MnPO_4$ crystallizes in a structure with space group (SG) Cmcm (# 63). One of the early experimental studies back in 1956 reported two additional sister structures of $MnPO_4$ (SG $P3_121$ and $I\bar{4}$) [32]. However, Cmcm is energetically the most stable structure (see Table I) and hence our choice for further calculations. The optimized lattice parameters of $MnPO_4$ in this structure (in primitive cell) is found to be $a = 4.711$ Å, $b = 4.711$ Å, and $c = 6.534$ Å. The crystal structure itself is shown in Fig. 1(a), which contains two formula units with a total of 12 atoms in the unit cell. Figure 1(b) shows the corresponding hexagonal-shaped BZ. Dynamical stability of $MnPO_4$ (in this structure) has been verified by simulating the phonon dispersion, which does not show any imaginary phonon modes, as shown in Fig. 1(c).

TABLE I. Relative energies (ΔE) of $MnPO_4$ with different space groups (SG). Energy for Cmcm is taken as reference.

Space groups	ΔE (meV/atom)
Cmcm	0.0
$P3_121$	70.0
$I\bar{4}$	121.0

B. Electronic structure

We simulated different magnetic ordering of Mn in $MnPO_4$, such as ferromagnetic (FM), antiferromagnetic (AFM), and a few ferrimagnetic configurations using 2 × 1 × 1 supercell, which contains 4 Mn atoms (see SM [33] for more details). Among these, FM turns out be energetically the most stable one. The magnitude of exchange interactions between neighboring Mn atoms lie in the range ∼5–11 meV. We have also obtained a rough estimate of the Curie temperature, which turns out to be ∼505 K, implying a FM to paramagnetic transition. Figure 1(d) shows the spin-polarized band structure and density of states (without SOC) of $MnPO_4$ in the FM phase. It clearly confirms the SGS behavior where one spin channel is semiconducting while the other has a zero gap. The spin-up band structure shows an elliptical nodal ring-type dispersion centering around the Y point in BZ. However, there are tiny gap openings on the nodal ring along Y-Γ direction. Figure 2(a) shows the orbital projected band structure including the effect of SOC. The insets show a zoomed view at/near the nodal points. Inclusion of SOC does not change the band topology much but slightly enhances the energy gap along the nodal ring. Such small gap openings along the nodal ring have earlier been observed in many systems, e.g., ZrSiS [34,35], Cu_3PdN [36,37], TiB_2 [38], CaPd [39], CaAgBi [40], etc. In

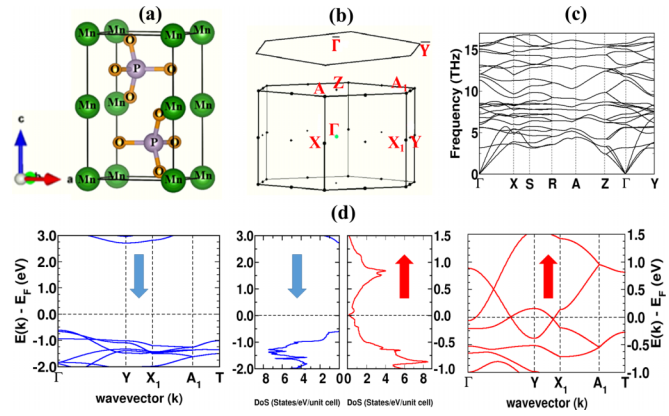

FIG. 1. For $MnPO_4$ (a) crystal structure with space group Cmcm (# 63). (b) BZ for bulk and (001) surface. (c) Phonon dispersion. (d) Spin polarized band structure and density of states (DoS) without spin-orbit coupling (SOC).

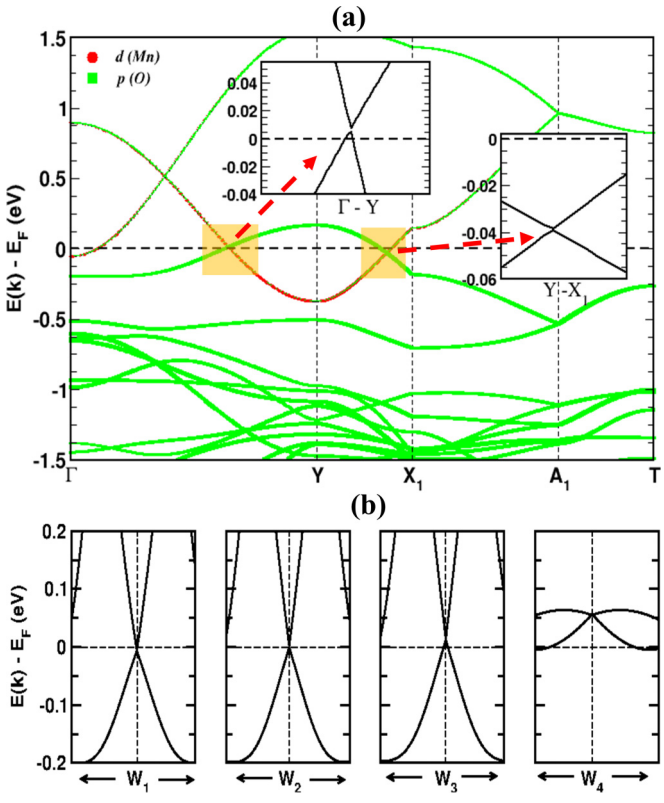

FIG. 2. (a) Orbital projected band structure of $MnPO_4$ with SOC, indicating two topological nodal points, one along Γ-Y and the other along Y-X_1 high symmetry points. A zoomed view around the nodal points are shown in the insets. (b) Dispersion around four positive chiral Weyl nodes, $W^{+}_{i=1,2,3,4}$, with Chern number $+1$. The dispersion around Weyl node with negative Chern number looks very similar.

the present case, the nodal ring is formed due to the band inversion between oxygen p orbital and Mn-d orbital at/near Y point.

Being ferromagnetic in nature, $MnPO_4$ lacks TRS and hence expected to contain Weyl-like twofold degenerate band crossings at a generic K point in the BZ. Unlike other conventional Weyl semimetals, ferromagnetic $MnPO_4$ shows four pairs of Weyl nodes. Table II shows the reciprocal space coordinates and the respective chiralities of these nodes. Interestingly, three pairs of these nodes, $(W^{\pm}_i; i = 1, 2, 3)$ lie on $k_z = 0$ plane, while the fourth one $(W^{\pm}_4)$ on $k_z = \pm 0.233$ plane. The total topological charge associated with these eight Weyl nodes sum up to zero, which is in accordance with the Nielsen-Ninomiya theorem [41]. Eight Weyl points and nodal loop are marked in the BZ, and presented in supplemental Fig. S2. Figure 2(c) shows the band dispersion near these four Weyl nodes.

TABLE II. Weyl points location in the BZ and their respective chiralities. $W^{\pm}_i$ represent ith Weyl point with chirality ± 1.

Weyl points	Coordinates (k_x, k_y, k_z)	Chirality
W^{+}_1	(0.302,−0.404, 0.000)	+1
W^{-}_1	(−0.302, 0.404, 0.000)	−1
W^{+}_2	(0.381, −0.30, 0.000)	+1
W^{-}_2	(−0.385, 0.30, 0.000)	−1
W^{+}_3	(−0.334, 0.311, 0.000)	+1
W^{-}_3	(0.338, −0.308, 0.000)	−1
W^{+}_4	(−0.499, 0.499, 0.233)	+1
W^{-}_4	(0.499, −0.499, −0.233)	−1

C. Surface states

Surface states are one of the most enlightening features of a topological quantum material. Based on the multifaceted nature of the Weyl nodes in the bulk, $MnPO_4$ is expected to host rich surface states. We have analyzed the projected (001)-surface band structures. Due to the nodal line-type behavior of the bulk electronic structure, a drumheadlike unique surface state appears when the nodal loop is projected on the (001) surface. The corresponding surface states and Fermi surface topology are presented in Figs. 3(a), 3(b). As evident from Fig. 3(a), bright surface states (drumheadlike) are clearly distinguishable from the bulk counter part. Also Fermi surface at an isoenergy of E_F display the elliptical nodal ring on the (001) surface as expected [see Fig. 3(b)]. Further, since nodal ring breaks down under the influence of SOC with a subsequent appearance of Weyl nodes, one should also expect the emergence of surface states from the Weyl points. The surface dispersions near $W_{i=1,2,3}$ Weyl nodes are simulated on the (001) surface, while that for W_4, it is performed on the (010) surface. This is becaue the projection of W_4 on (001) surface aligned very close to the Y point. These surface dispersions are shown in Figs. 3(c)–3(f). One can observe the bright surface states emerging from each of these nodes as well. The Fermi arcs arising out of these Weyl points are, however, not seen on the (001) surface since they are submerged within the bulk spectral density.

D. Anomalous Hall effect

A magnetic Weyl semimetal is often characterized by its transverse conductivity. Here, we have examined the AHC of $MnPO_4$ in a wide range of energy span. Since the magnetization of the compound is oriented along the z direction, the principal transport parameter to analyze here is σ_{xy}. We have computed the anomalous Hall conductivity from Berry curvature, using the following relation:

$$\sigma_{\alpha\beta} = -\frac{e^2}{\hbar}\int_{BZ}\frac{d^3k}{(2\pi)^3}\Omega_{\alpha\beta}(k).$$

Figure 4(a) shows the energy dependence of AHC for ferromagnetic $MnPO_4$. There are few important energy ranges where the variation/magnitude of AHC is quite interesting and hence require a discussion. Between -0.5 to $+0.5$ eV, σ_{xy} is almost negligible, which increases to 100 Ω^{-1} cm^{-1} in the range -1.0 to -0.6 eV, and further to 220 Ω^{-1} cm^{-1} at around -0.8 eV. These later values of σ_{xy} are comparable with the corresponding reported values in several Heusler alloys [42–44]. Most promisingly, we have observed a peak in σ_{xy} at around -1.37 eV with the largest magnitude of 1265 Ω^{-1} cm^{-1}. Generally, such peaks in AHC are expected to occur at an energy (E_F in the case of $MnPO_4$) where Weyl points occur. However, in the present case, it is occurring somewhat

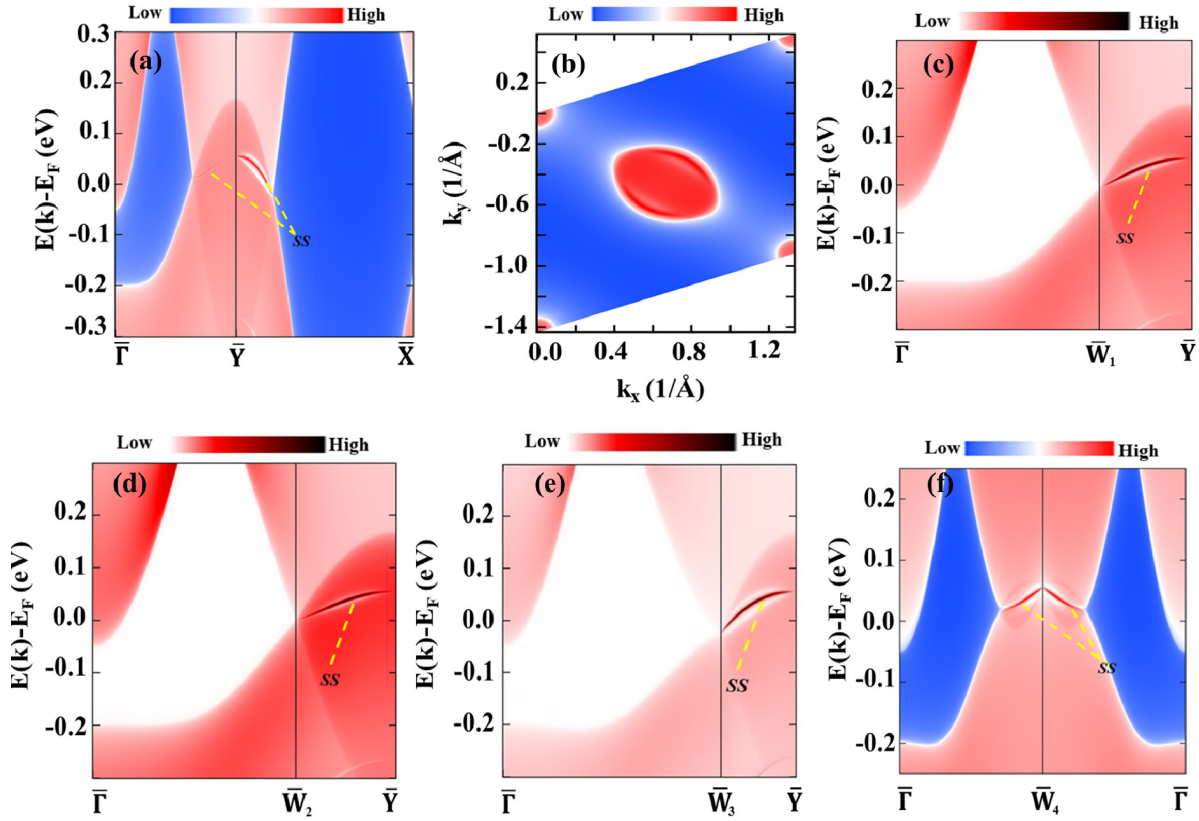

FIG. 3. Surface band structure of $MnPO_4$. (a) Electronic dispersion on the (001) surface around Y point in the BZ. SS indicates drumheadlike surface states arising out of nodal ring, (b) Fermi surface topology on (001) surface. (c)–(e) Dispersion on (001) surface around three Weyl nodes, $\overline{W}_{i=1,2,3}$, (f) Dispersion on (010) surface of W_4.

away from the E_F. Such behavior is reported in few other materials as well in the past [45,46]. To better understand this feature of AHC, a close inspection of electronic structure is essential. One plausible reason for such behavior is the lack of large density of states near E_F [see Fig. 4(a) bottom panel], which can eventually provide a decremental effect on both Berry curvature and AHC [47]. Apart from this, we further plotted the z component of Berry curvature in Fig. 4(b). Here, light yellow color represents positive hot spot, and dark brown represents the negative hot spot, and from Fig. 4(b), one can clearly see the lower magnitude of Berry curvature.

The percentage of spin polarization also influences the net magnitude of AHC in weak SOC systems [48,49]. The total AHC (σ^t_{xy}) can be written as the sum of σ_{xy} (spin up) and σ_{xy} (spin down) at specific chemical potential [48,49]. For our proposed compound $MnPO_4$, a 100% spin polarization is observed at E_F, which remains preserved for a wide energy range of -0.6 to $+2.7$ eV. This actually suppresses the AHC values. Below -0.6 eV, one can clearly see the mixture of spin-up and spin-down states, causing an enhanced value of AHC. A similar trend has been reported in few Co-based Heusler alloys [45,46]. It is clearly evident from the above discussion that $MnPO_4$ is indeed a promising candidate for future spintronic application. It can even become promising for topological materials related applications if one can tune the position of Fermi level by doping or external pressure/strain without much compromising the band profile.

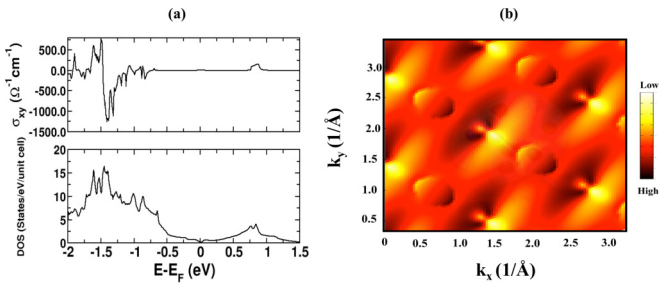

FIG. 4. (a) Anomalous Hall conductivity (top), density of states (bottom), including SOC contribution. (b) z component of Berry curvature at E_F on the k_x-k_y plane.

IV. SUMMARY

In summary, we report the coexistence of two complementary quantum phenomena, namely spin-gapless semiconducting (SGS) behavior and topologically nontrivial multi-Weyl Fermions, in a single compound $MnPO_4$. Materials with such coexistent phenomenon are called composite quantum compounds (CQC). SGSs are a special class of spintronic materials, which acquire a unique band structure with one spin channel showing semiconducting nature while the other shows a gapless state (similar to graphene). Our detailed band structure calculations unfold the existence of SGS as well as

four distinct pairs of Weyl nodes in the bulk electronic dispersion of $MnPO_4$. Interestingly, these Weyl nodes are located very close to the Fermi level with the minimal trivial band density. The chirality of these Weyl nodes are confirmed by calculating their respective topological charges. We found the so-called drumheadlike nodal line surface states on the (001) surface. Such coexistent topological semimetallic signature along with the SGS behavior in $MnPO_4$, will definitely attract further research interests in the field of spintronics and topological nontrivial materials.

ACKNOWLEDGMENTS

A.A. acknowledges DST SERB, India (Grant No. CRG/2019/002050) for funding to support this research. P.C.S. and C.K.B. thank IIT Bombay space time computing facility, and Dr. Debashish Das for helpful discussions. F.-C.C. acknowledges support from National Center for Theoretical Sciences and the Ministry of Science and Technology of Taiwan under Grant No. MOST-107-2628-M-110-001-MY3. He is also grateful to the National Center for High-performance Computing for computer time and facilities.

[1] J. Li, Y. Li, S. Du, Z. Wang, B-L. Gu, S.-C. Zhang, K. He, W. Duan, and Y. Xu, Science Advances **5**, eaaw5685 (2019).
[2] M. Z. Hasan and C. L. Kane, Rev. Mod. Phys. **82**, 3045 (2010).
[3] X. L. Qi and S. C. Zhang, Rev. Mod. Phys. **83**, 1057 (2011).
[4] C. Liu, Y. Wang, H. Li, Y. Wu, Y. Li, J. Li, K. He, Y. Xu, J. Zhang, and Y. Wang, Nature Mater. **19**, 522 (2020).
[5] Y. S. Hou, J. W. Kim, and R. Q. Wu, Phys. Rev. B **101**, 121401(R) (2020).
[6] D. DiSante, P. Barone, A. Stroppa, K. F. Garrity, D. Vanderbilt, and S. Picozzi, Phys. Rev. Lett. **117**, 076401 (2016).
[7] X. Xi, C. Ma, Z. Liu, Z. Chen, W. Ku, H. Berger, C. Martin, D. B. Tanner, and G. L. Carr, Phys. Rev. Lett. **111**, 155701 (2013); M. S. Bahramy, B. J. Yang, R. Arita, and N. Nagaosa, Nature Commun. **3**, 679 (2012).
[8] S. Ouardi, G. H. Fecher, C. Felser, and J. Kubler, Phys. Rev. Lett. **110**, 100401 (2013); X. L. Wang, *ibid.* **100**, 156404 (2008).
[9] S. Skaftouros, K. Özdoğan, E. Şaşıoğlu, and I. Galanakis, Appl. Phys. Lett. **102**, 022402 (2013).
[10] J. Han, Y. Feng, K. Yao and G. Y. Gao, Appl. Phys. Lett. **111**, 132402 (2017).
[11] A. Kundu, S. Ghosh, R. Banerjee, S. Ghosh, and B. Sanyal, Sci. Rep. **7**, 1803 (2017).
[12] D. Rani Enamullah, L. Bainsla, K. G. Suresh, and A. Alam, Phys. Rev. B **99**, 104429 (2019); D. Rani, L. Bainsla, A. Alam, and K. G. Suresh, J. Appl. Phys. **128**, 220902 (2020); L. Bainsla, A. I. Mallick, M. M. Raja, A. K. Nigam, B. S. D. C. S. Varaprasad, Y. K. Takahashi, A. Alam, K. G. Suresh, and K. Hono, Phys. Rev. B **91**, 104408 (2015); L. Bainsla, A. I. Mallick, M. M. Raja, A. A. Coelho, A. K. Nigam, D. D. Johnson, A. Alam, and K. G. Suresh, *ibid.* **92**, 045201 (2015).
[13] N. Nagaosa, J. Sinova, S. Onoda, A. H. MacDonald, and N. P. Ong, Rev. Mod. Phys. **82**, 1539 (2010).
[14] R. Shindou and N. Nagaosa, Phys. Rev. Lett. **87**, 116801 (2001).
[15] W. Shi, L. Muechler, K. Manna, Y. Zhang, K. Koepernik, R. Car, J. van den Brink, C. Felser, and Y. Sun, Phys. Rev. B **97**, 060406(R) (2018).
[16] E. Liu, Y. Sun, N. Kumar, L. Muechler, A. Sun, L. Jiao, S.-Y. Yang, D. Liu, A. Liang, Q. Xu, J. Kroder, V. S. Horst Borrmann, C. Shekhar, Z. Wang, C. Xi, W. Wang, W. Schnelle, S. Wirth, Y. Chen, S. T. B. Goennenwein, C. Felser, Nature Phys. **14**, 1125 (2018).
[17] J. Shen, Q. Zeng, S. Zhang, H. Sun, Q. Yao, X. Xi, W. Wang, G. Wu, B. Shen, Q. Liu, and E. Liu, Adv. Funct. Mater. **30**, 2000830 (2020).
[18] P. Li, J. Koo, W. Ning, J. Li, L. Miao, L. Min, Y. Zhu, Y. Wang, N. Alem, C.-X. Liu, Z. Mao, B. Yan, Nature Commun. **11**, 3476 (2020).
[19] B. M. Ludbrook, B. J. Ruck, and S. Granville, Appl. Phys. Lett. **110**, 062408 (2017).
[20] J. Shen, Q. Yao, Q. Zeng, H. Sun, X. Xi, G. Wu, W. Wang, B. Shen, Q. Liu, and E. Liu, Phys. Rev. Lett. **125**, 086602 (2020).
[21] S. Roy, R. Singha, A. Ghosh, A. Pariari, and P. Mandal, Phys. Rev. B **102**, 085147 (2020).
[22] G. Wang, Z. Sun, X. Si, and S. Jia, Chin. Phys. B **29**, 077503 (2020).
[23] G. Kresse and J. Hafner, Phys. Rev. B **47**, 558(R) (1993).
[24] G. Kresse and D. Joubert, Phys. Rev. B **59**, 1758 (1999).
[25] S. L. Dudarev, G. A. Botton, S. Y. Savrasov, C. J. Humphreys, and A. P. Sutton, Phys. Rev. B **57**, 1505 (1998).
[26] P. E. Blöchl, Phys. Rev. B **50**, 17953 (1994).
[27] A. Togo and I. Tanaka, Scr. Mater. **108**, 1 (2015).
[28] N. Marzari and D. Vanderbilt, Phys. Rev. B **56**, 12847 (1997).
[29] I. Souza, N. Marzari, and D. Vanderbilt, Phys. Rev. B **65**, 035109 (2001).
[30] N. Marzari, A. A. Mostofi, J. R. Yates, I. Souza, and D. Vanderbilt, Rev. Mod. Phys. **84**, 1419 (2012).
[31] QuanSheng Wu, ShengNan Zhang, Hai-Feng Song, Matthias Troyer, and A. A. Soluyanov, Comput. Phys. Commun. **224**, 405 (2018).
[32] E. C. Shafer, M. W. Shafer, and R. Roy, Z. Kristallogr., Bd. **108**, 263 (1956).
[33] See Supplemental Material at http://link.aps.org/supplemental/10.1103/PhysRevB.103.195143 for more details.
[34] L. M. Schoop, Mazhar N. Ali, C. Straßer, A. Topp, A. Varykhalov, D. Marchenko, V. Duppel, Stuart S. P. Parkin, Bettina V. Lotsch, and Christian R. Ast, Nature Commun. **7**, 11335 (2016).
[35] M. Neupane, I. Belopolski, M. M. Hosen, D. S. Sanchez, R. Sankar, M. Szlawska, S. Y. Xu, K. Dimitri, N. Dhakal, P. Maldonado, P. M. Oppeneer, D. Kaczorowski, F. Chou, M. Z. Hasan, and T. Durakiewicz, Phys. Rev. B **93**, 201104(R) (2016).
[36] Youngjuk Kim, B. J. Wieder, C. L. Kane, and A. M. Rappe, Phys. Rev. Lett. **115**, 036806 (2015).
[37] R. Yu, H. Weng, Z. Fang, X. Dai, and X. Hu, Phys. Rev. Lett. **115**, 036807 (2015).
[38] Z. Liu, Rui Lou, Pengjie Guo, Qi Wang, Shanshan Sun, Chenghe Li, Setti Thirupathaiah, Alexander Fedorov, Dawei Shen, Kai Liu, Hechang Lei, and Shancai Wang, Phys. Rev. X **8**, 031044 (2018).
[39] G. Liu, Lei Jin, X. Dai, G. Chen, and X. Zhang, Phys. Rev. B **98**, 075157 (2018).

[40] A. Yamakage, Y. Yamakawa, Y. Tanaka, and Y. Okamoto, J. Phys. Soc. Jpn. **85**, 013708 (2016).
[41] H. B. Nielsen and M. Ninomiya, Phys. Lett. B **105**, 219 (1981).
[42] A. Husmann and L. J. Singh, Phys. Rev. B. **73**, 172417 (2006).
[43] B. K. Hazra, M. Manivel Raja, R. Rawat, A. Lakhani, S. N. Kaul, and S. Srinath, J. Magn. Magn. Mater. **448**, 371 (2018).
[44] J. Kudrnovský and V. Drchal, I. Turek, Phys. Rev. B. **88**, 014422 (2013).
[45] C. S. Spencer, J. Gayles, N. A. Porter, S. Sugimoto, Z. Aslam, C. J. Kinane, T. R. Charlton, F. Freimuth, S. Chadov, S. Langridge, J. Sinova, C. Felser, S. Blügel, Y. Mokrousov, and C. H. Marrows, Phys. Rev. B **97**, 214406 (2018).
[46] Kaustuv Manna, Yan Sun, Lukas Muechler, J. Kübler, and C. Felser, Nature Rev. Mater. **3**, 244 (2018).
[47] E. I. Kondorskii, Zh. Eksp. Teor. Fiz. **55**, 558 (1968).
[48] K. Manna, L. Muechler, T. H. Kao, R. Stinshoff, Y. Zhang, J. Gooth, N. Kumar, G. Kreiner, K. Koepernik, R. Car, J. Kubler, G. H. Fecher, C. Shekhar, Y. Sun, and C. Felser, Phys. Rev. X **8**, 041045 (2018).
[49] T. Jen-Chuan and G. Guang-Yu, New J. Phys. **15**, 033014 (2013).